Eur. Phys. J. Appl. Phys. **51**, 10502 (2010)
DOI: 10.1051/epjap/2010071

THE EUROPEAN PHYSICAL JOURNAL APPLIED PHYSICS

Regular Article

Structural, optical and nanomechanical properties of (1 1 1) oriented nanocrystalline ZnTe thin films

M.S.R.N. Kiran[1], S. Kshirsagar[2], M.G. Krishna[2,3,a], and Surya P. Tewari[2,3]

[1] Department of Materials Engineering, Indian Institute of Science, Bangalore, India
[2] Advanced Centre of Research in High Energy Materials (ACRHEM), University of Hyderabad, Hyderabad, India
[3] School of Physics, University of Hyderabad, Hyderabad, India

Received: 19 February 2010 / Accepted: 3 May 2010
Published online: 17 June 2010 –

Abstract. Structural, optical and nanomechanical properties of nanocrystalline Zinc Telluride (ZnTe) films of thickness upto 10 microns deposited at room temperature on borosilicate glass substrates are reported. X-ray diffraction patterns reveal that the films were preferentially oriented along the (1 1 1) direction. The maximum refractive index of the films was 2.74 at a wavelength of 2000 nm. The optical band gap showed strong thickness dependence. The average film hardness and Young's modulus obtained from load-displacement curves and analyzed by Oliver-Pharr method were 4 and 70 GPa respectively. Hardness of (1 1 1) oriented ZnTe thin films exhibited almost 5 times higher value than bulk. The studies show clearly that the hardness increases with decreasing indentation size, for indents between 30 and 300 nm in depth indicating the existence of indentation size effect. The coefficient of friction for these films as obtained from the nanoscratch test was ∼0.4.

1 Introduction

Zinc telluride (ZnTe) is one of the important II-VI compound semiconducting materials which have potential applications in a variety of solid-state devices such as solar cells, photodetectors, light emitting diodes and Terahertz generators and detectors [1–3]. ZnTe is a zincblende electro-optic crystal in the far infrared range, but also has the largest emission efficiency and nearly the highest frequency bandwidth in the mid-infrared range [4]. Leitenstorfer et al. [5] have reported that the thickness of the electro-optic crystals is a crucial factor influencing the temporal wave form and spectral bandwidth of the measured THz pulse. In order to achieve broad frequency bandwidth, ZnTe crystals with thickness less than 10 μm are required. It is almost impossible to prepare self-supporting crystals with a large diameter and such low thicknesses. Therefore, it is extremely important to fabricate high-quality ZnTe thick films of the order of 10 μm or greater, directly on to appropriate substrates with large size.

There are several reports on deposition of polycrystalline ZnTe thin films by various techniques [6–15]. Most of the previous research has focused primarily on the structural, electrical and optical properties of ZnTe both in the form of bulk crystals and sub-micron thin films [16–20]. Limited attention has been paid to the mechanical properties of ZnTe thin films. Mechanical properties assume importance especially in the case of thick films since surface layers of these films may be exposed to external mechanical effects including wear, damage and thermal degradation [21]. Recently, nanoindentation techniques have been employed extensively to quantify the mechanical properties of thin films [22–25] such as hardness, elastic modulus and adhesion. Among these, the adhesion of coatings to the substrates is a key factor for the mechanical behavior of coated parts [24]. In addition, the grain size and grain morphologies have a direct influence on the mechanical properties of the films.

In this work, we present results on the preparation and characterization of ZnTe films deposited on to borosilicate glass substrates using the thermal evaporation technique. The films were characterized for structure, optical and nanomechanical properties.

2 Experimental

ZnTe thin films of different thicknesses were deposited by evaporating pure ZnTe compound (99.995%, supplied by Aldrich Chemicals) onto cleaned borosilicate glass substrates at ambient temperature. The ultimate vacuum of about 6×10^{-6} mbar was reached using a diffusion pump backed by a rotary pump. The glass substrates were cleaned using detergent solution, followed by multiple rinsing in distilled water to remove traces of detergent. The substrates were then cleaned in an ultrasonic cleaner for 15 min and subsequently dried in flowing hot air.

[a] e-mail: mgksp@uohyd.ernet.in

The evaporation rate as well as the film thickness was controlled using a quartz crystal monitor. The distance between the source and substrate was maintained at 5 cm for all the experiments. Deposition time, evaporation currents have been varied to make films of different thicknesses. The thickness of the films was determined by a surface profilometer (XP-1 of Ambios Technology, USA). The structure of the films was determined using a powder X-ray diffractometer (Philips PW3710) equipped with a position-sensitive detector using Cu K_α (=1.5418 Å) radiation. Spectral transmittance curves of the films were recorded in a UV–VIS–NIR spectrophotometer (Model V-570 of JASCO International, Japan), scanning from 300 to 2500 nm. The optical properties, i.e. refractive index and band gap of the film, were derived from the spectral transmission curves. The surface topography, microstructure, grain area analysis and particle size were investigated by using an Atomic Force Microscope (SPA-400 of SII, Inc. Japan), operating in the intermittent contact dynamic force mode. The root mean square (rms) roughness was calculated over a 2 μm $\times$ 2 μm scan area.

Indentation experiments were performed using a Triboscope® Nanomechanical Testing System (Hysitron Inc., Minneapolis, MN). The system was fitted with a Berkovich indenter (three-sided pyramid shape tip). Prior to the nanoindentation experiments, the tip area function was calibrated by performing few nano-indentation experiments on fused silica. The calibration method is based on the assumption that Young's modulus of elasticity is independent of indentation depth. Thus, fused silica, which has a relatively constant Young's modulus (69.6 GPa), is used as a standard sample for calibration. To determine the area function, a series of indents were introduced at various contact depths. The contact areas were then calculated using empirical equations for the Berkovich tip. A plot of the computed area versus contact depth was then obtained. By fitting this plot with a high order polynomial, an area function relating the projected contact area to the contact depth was obtained for the Berkovich tip that was used. The hardness of a material is defined as its resistance to local plastic deformation [26,27]. Thus, the hardness, H, could be determined from the maximum indentation load, $P_{\max}$, divided by the contact area, i.e.

$$H = \frac{P_{\max}}{A} \tag{1}$$

where the contact area (A) is a function of the penetration depth, h, and can be determined according to equation (2)

$$A(h) = C_0h^2+C_1h+C_2h^{1/2}+C_3h^{1/4}+\ldots+C_8h^{1/128}. \tag{2}$$

This was used as the calibrated area function in subsequent experiments on ZnTe films. It may be noted that only the constant C_0 is used, if it is assumed that a Berkovich indenter has a perfect tip. However for imperfect tips, higher order terms have to be taken into account and these are obtained from the tip area function curve fit for a given tip. In the current case, the values are $C_0 = 24.5$, $C_1 = -2.2025 \times 10^3$, $C_2 = 2.158 \times 10^5$, $C_3 = -1.7098 \times 10^6$, $C_4 = -3.4482 \times 10^6$ and $C_5 = -1.9066 \times 10^6$. The Young's modulus, E, of the thin film, can be obtained using equation (3)

$$\frac{1}{E_r^*} = \frac{1-\nu_i^2}{E_i} + \frac{1-\nu_s^2}{E_s} \tag{3}$$

where ν and E are Poisson's ratio and Young's modulus, respectively, and the subscripts i and s refer to the indenter and test material. The indenter properties used in this study are $E_i = 1140$ GPa, Poisson's ratio for the indenter is $\nu_i = 0.07$. E_r^* is the effective elastic modulus and it can be determined from the equation

$$E_r^* = \frac{\sqrt{\pi}}{2}\,\frac{\beta S}{\sqrt{A}} \tag{4}$$

where S is the stiffness of the test material, which can be obtained from the initial unloading slope by evaluating the maximum load and the maximum depth, i.e. $S = \mathrm{d}P/\mathrm{d}h$. β is a shape constant that depends on the geometry of the indenter and is 1.034 for the Berkovich tip.

During the test, contact mode AFM scans were obtained before and after each indentation. A load-depth curve was also recorded for each indent. The tests were conducted under load control, using peak loads in the range between 200 μN and 10 mN. A partial unload function is used in this experiment. A loading rate of 50 μN/s was used for all the experiments. A hold period of 10 s was applied at peak loads. After 10 s hold, unloading (upto 50% of peak load) starts with an unloading rate of 50 μN/s. The hold periods were used to allow time dependent plastic effects to diminish. In this way, the loading curves obtained for various peak loads were found to exhibit good reproducibility. This type of load function is useful to find out where exactly the elastic-plastic transformation occurs and also to obtain depth dependent mechanical properties. To find out coefficient of friction of ZnTe films, nanoscratch test was performed. A ramp force (normal force increases with time) scratch mode was used in this study. A 6 micron length scratch made on films with a normal force varied from 0 to 1000 μN in 30 s.

3 Results and discussion

ZnTe coatings were deposited for different durations to observe the evolution of the film thickness at a rate of deposition of 400 nm/min. The film thickness increased with increasing growth time. In this process, it was found that beyond a critical thickness (~4 micron), films delaminated from the substrate. To overcome this problem, deposition rate was decreased to 300, 200 and 100 nm/min and the time of deposition increased. This process increased the critical thickness for peel-off to 6 and 9 micron, for the rate of deposition of 300 and 200 nm/min, respectively. Figure 1 shows a typical X-ray diffraction profile of the ZnTe film grown on amorphous glass substrate. Only crystalline peaks from (1 1 1) orientation ZnTe were observed. Due to the very high film thickness, amorphous

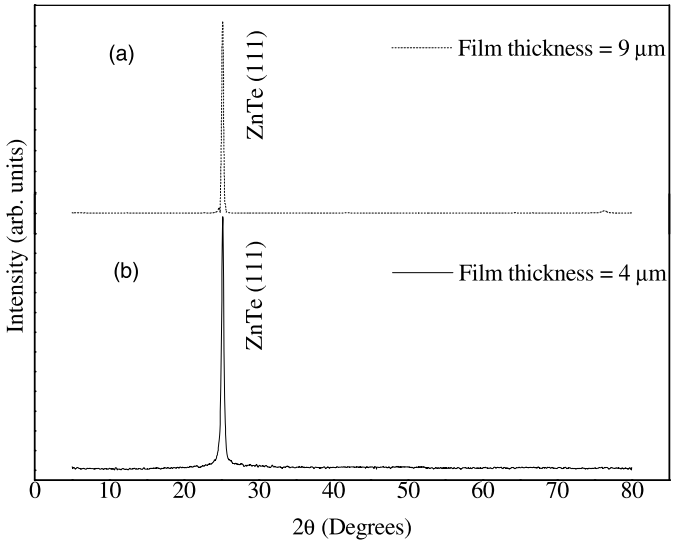

Fig. 1. X-ray diffraction of ZnTe thin films of different thicknesses (a) 9 μm and (b) 4 μm reveals that the films are oriented in (1 1 1) orientation.

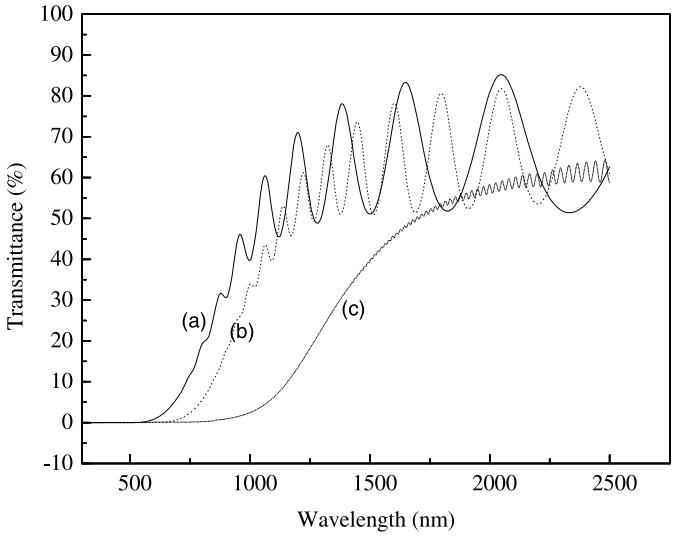

Fig. 2. Measured spectral transmission curves of ZnTe thin films at different thicknesses (a) 1.5 (b) 4, and (c) 10 μm.

glassy background was not observed in the X-ray diffraction pattern. The lattice constant obtained from the (1 1 1) peak for the ZnTe layer, is 6.1 Å, which is in good agreement with the reported values. The crystallite size of the films was 40 nm, calculated using Scherrer's formula. Very recently, Shaaban et al. [28] have deposited ZnTe films at various thicknesses i.e. from 300 to 600 nm on glass substrates by thermal evaporation technique. But their X-ray diffraction reveals that the films are polycrystalline of zinc-blende structure with peaks at $2\theta = 25.42°$, 42.20°, 49.87° and 67.14° corresponding to (1 1 1), (2 2 0), (3 1 1) and (3 3 1) orientations, respectively. (JCPDS Data file: 01-0582-cubic.) In the present case, a combination of rate of deposition and the film thickness played a major role in the evolution of (1 1 1) orientation in the films.

Figure 2 illustrates that the typical measured spectral transmittance curves of ZnTe films of three different thicknesses. The refractive index was determined using Swanpoel's method [29,30]. According to this method, the value of refractive index of the film, n, at a wavelength λ can be calculated using the following expression:

$$n = \left[N + (N^2 - s^2)^{1/2}\right]^{1/2} \tag{5}$$

where

$$N = 2s\frac{T_M - T_m}{T_M T_m} + \frac{s^2 + 1}{2}. \tag{6}$$

Here T_M and T_m are the transmittance maximum and the corresponding minimum at a certain wavelength λ and s is the refractive index of the substrate at that wavelength.

The thickness of the films in Figures 2a–2c were 1.5, 4.0 and 10 μm respectively and the corresponding refractive indices at a wavelength of 2000 nm were 2.74, 2.6 and 1.80 respectively.

For an optically homogeneous film the refractive index is constant across the thickness of a film at a given wavelength. This is manifested in the form of fringes of constant height in the dispersion free region of the refractive index. However, for an optically inhomogeneous film the dispersion in refractive index is thickness dependent and this is inferred from the variable fringe height in the measured spectral transmittance curve for such a film. It is evident that all the films in the current study are optically inhomogeneous. The origins of inhomogeneity can either be chemical or microstructural in nature. Chemical inhomogeneity leading to optical inhomogeneity in thermally evaporated ZnTe thin films has been reported earlier [31]. Since Zn has a higher vapour pressure than Te, films tend to be Zn rich upto a certain thickness and stoichiometric thereafter. This non-stoichiometry may be below the detectable limits of X-ray diffraction in the current study. Thin films deposited by thermal evaporation normally exhibit a columnar microstructure with a thickness dependent diameter of columns causing variable porosity in the films, across their thickness. This, in turn, leads to variations in refractive index across the thickness and therefore optical inhomogeneity. A further consequence of the columnar microstructure is, especially at higher thicknesses, increased scattering of light due to loss of coherence between the primary beam and the beam reflected between the film boundaries resulting in the disappearance of the interference which in turn decreases the total transmission from the film.

In the vicinity of the fundamental absorption edge, for allowed direct band-to-band transitions, the absorption coefficient is described by the

$$\alpha(h\nu) = \frac{K\left(h\nu - E_g^{opt}\right)^m}{h\nu} \tag{7}$$

where K is a characteristic parameter (independent of photon energy) for respective transitions, $h\nu$ denotes photon energy, is E_g^{opt} optical energy gap and m is a number which characterizes the transition process. Different

authors [32–34] have suggested different values of m for different glasses, $m = 2$ for most of the amorphous semiconductors (indirect transition) and $m = 1/2$ for most of the crystalline semiconductor (direct transition). In the case of different thicknesses of polycrystalline ZnTe thin films the direct transition is valid. The optical bandgap value for (1 1 1) oriented ZnTe films exhibited 2.6, 1.9 and 1.33 eV for the films shown in Figures 2a–2c, respectively. It is evident that the increase in thickness leads to a decrease in optical absorption edge/bandgap, as observed in oxides and nitrides earlier [35,36]. Defects in thin films originate during the formation of the films, thus unsaturated bonds can be produced as a result of an insufficient number of atoms being present. These bonds are responsible for the formation of some defects producing localized states in the films. The thicker films increase the width of the localized states in the optical absorption edge or band gap; consequently the optical absorption edge decreases with increase in thickness [37]. The deviation in the band gap can also be due to the excess of unbound Te present in the ZnTe films. The presence of elemental Te introduces a significant fraction of electronic levels in the band gap close to the valence band edge of ZnTe, with a consequent reduction of the energy associated with the direct transition [38].

The microstructure of ZnTe films is shown in Figure 3. AFM micrographs reveal that the particle size for the film of thickness 4 μm was 160 nm, whereas it increased to 380 nm for the film of thickness 10 μm. The root mean square roughness of the films was 0.4 and 3.3 nm for the films of thickness 4 and 10 μm, respectively. It can be seen from the films that the 10 μm thick films showed a larger particle size distribution than the 4 μm films. This indicates a thickness dependent grain growth in the coatings.

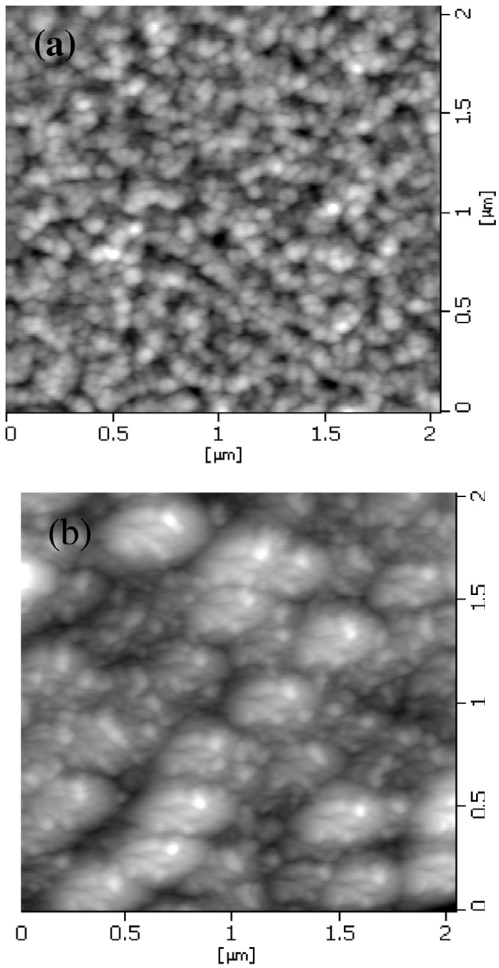

Fig. 3. Atomic Force Microscope images of ZnTe films of (a) 4 and (b) 10 μm thickness.

The hardness and modulus of the films were calculated using Oliver and Pharr analysis [39,40]. The reported microhardness value of bulk ZnTe crystal was 900 ± 50 MPa [41] and 3.5 GPa for 1.2 μm thick ZnTe layers [42]. For the films in the current study, the highest hardness of 4 GPa and modulus of 70 GPa were obtained. It can be noted that the hardness of the films were 5 times greater than the bulk ZnTe crystal. In order to measure the "film-only" properties, a commonly used rule is to limit the indentation depth to less than 10% of the film thickness [43]. Figure 4 shows that the value of hardness increases with decreasing the indentation depth. At lower depths the hardness reached an average value of 6 GPa and it decreased to 3.5 GPa at higher depths. This type of behaviour is known as indentation size effect (ISE). Increasing strength at small length scale (so called ISE) has been observed in many metallic systems [44]. Since conventional plasticity theories do not include any material length scales, they cannot be used to model indentation size effects in thin films with indents at the micron-scale and sub-micron scale, where the size effect is evident. Strain gradient plasticity theories [45,46] are, therefore, needed to explain the size effects. Nix and Gao [47] have developed a mechanism based strain gradient (MSG) model that can be used to explain the indentation size effects. The MSG theory assumes that the indentation is accommodated by circular loops of geometrically necessary dislocations (GNDs) with Burgers vectors normal to the plane surface. The model combines the Taylor relation [48], the Mises flow rule and the Tabor relation [48] to obtain the following characteristic expression for the depth dependence of hardness,

$$\frac{H}{H_0} = \sqrt{1 + \frac{h^*}{h}} \tag{8}$$

where H is the hardness for a given indent depth, h; H_0 the size independent hardness, and h^* is a characteristic length parameter that characterizes the depth dependence of the hardness. This model predicts that the square of the hardness should be linearly related to the reciprocal of the indentation depth. The linear relationship is in agreement with the plots of nano-indentation data obtained from the ZnTe nanocrystalline thin films (crystallite size ~40 nm) examined in this study. This is shown in Figure 5, in which linear relationships are obtained between $(H/H_0)^2$ and $1/h$, for (1 1 1) orientated nanocrystalline ZnTe thin films. The hardness H_0, of an infinitely large dislocation where

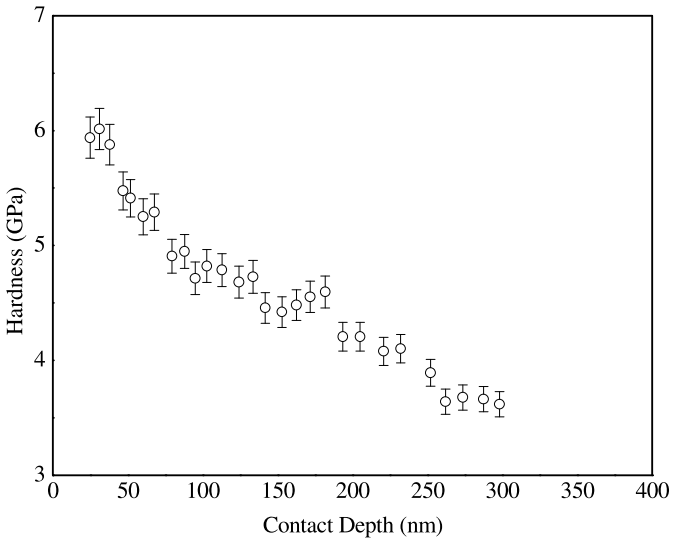

Fig. 4. Variation in hardness values of ZnTe films with increasing the contact depth of the Berkovich indenter.

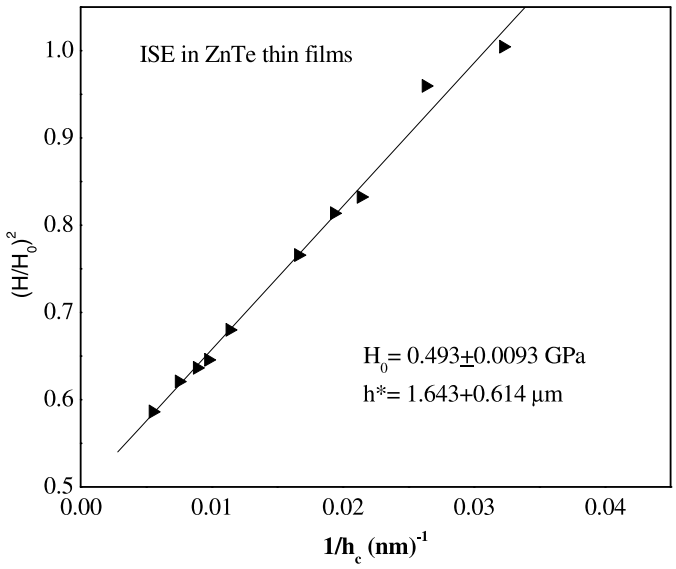

Fig. 5. The relationship between $(H/H_0)^2$ and $1/h$, for (1 1 1) orientated nanocrystalline ZnTe thin films, which is known as indentation size effect.

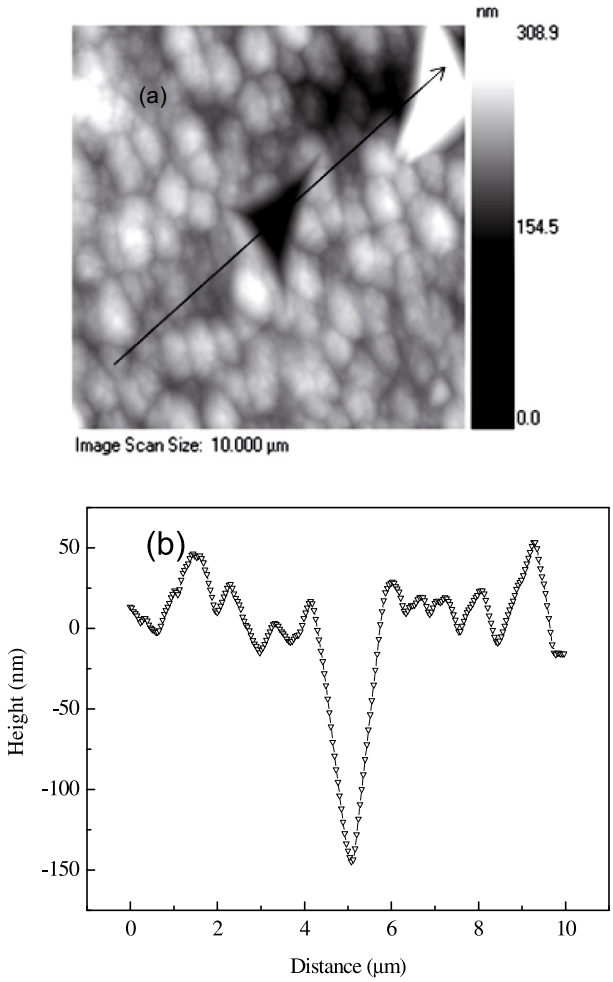

Fig. 6. (a) AFM image of residual Berkovich impression after removing the load. No pile-up and sink-in effects observed and were confirmed from this image. (b) Indent profile of the impression (direction shown with an arrow mark).

size effects are negligible is 0.493 GPa, obtained from the intercept of the line with the y-axis in Figure 5. h^*, which characterizes the depth dependence of the hardness as is obtained from the slope of the line in Figure 5, is 1600 nm. Since this is the first report on the existence of ISE in ZnTe films, we cannot compare our results with any other reports.

No substrate effects have been found on the behaviour of the hardness with increasing penetration depth. Even when the penetration depth is very large (max. 300 nm at 10 mN load), the composite hardness value never equals the substrate hardness value, which is 7 GPa for glass substrates. It may be due to the fact that most of the plastic deformation is limited in thin films. Interestingly, no pile-up or sink-in effects were observed after indentation revealed by the atomic force microscope images as shown in Figure 6a. The line profile, shown in Figure 6b, also reveals the absence of the pile-up and sink-in effects. No pop-in behaviour observed in the load- displacement data, which indicates the transition from elastic to plastic deformation due to the nucleation of dislocations. The average elastic modulus of the ZnTe films was 70 GPa, as shown in Figure 7. The coefficient of friction (COF), defined as the ratio of lateral force to normal force (LF/NF), has been calculated using the scratch test. The average COF obtained from the scratch test was 0.4 as shown in Figure 8. The AFM image of scratch on ZnTe films is shown in Figure 9a and the corresponding line profile along the scratch is shown in Figure 9b. The films adhere better with the substrate even for film of thickness 10 μm deposited on glass substrate without significant delamination. No material pile up observed on both sides of the scratch was found, though sharp Berkovich tip was used. This can be attributed to the higher film hardness.

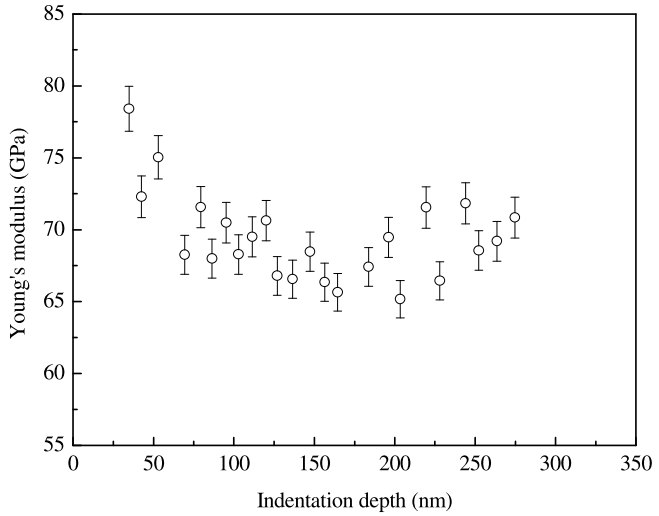

Fig. 7. The variation of Young's modulus of ZnTe films with increasing the contact depth of the Berkovich indenter.

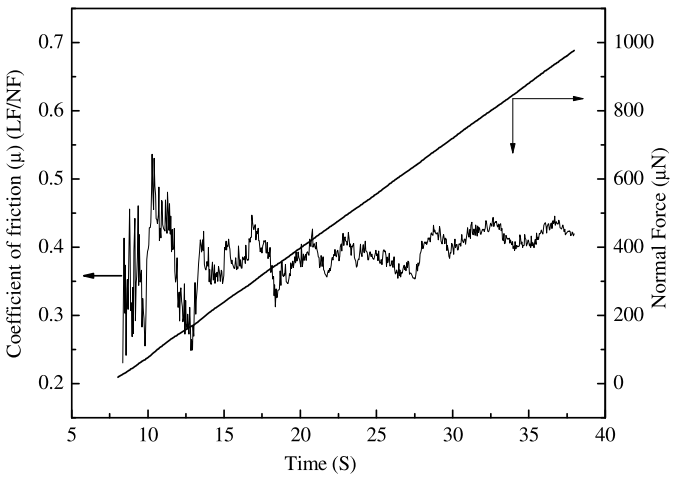

Fig. 8. The coefficient of friction of ZnTe films on glass substrate. This graph is obtained from the nanoscratch test using nanoindentation system in the scratch mode.

4 Conclusions

Zinc telluride (ZnTe) thin films oriented along the (1 1 1) direction have been deposited by resistive thermal evaporation technique. Films of thickness up to 10 μm have been realized without significant delamination. The optical bandgap value decreased with increasing film thickness. Nanomechanical hardness of the (1 1 1) oriented ZnTe films was 5 times higher than the bulk ZnTe crystal value. Significantly, indentation size effect was observed in the semiconducting (1 1 1) oriented ZnTe films.

The authors acknowledge the facilities provided under the UGC-CAS & UPE, and DST-ITPAR programs. Financial support in the form of fellowships to MSRNK and SK from the ACRHEM project of DRDO is acknowledged.

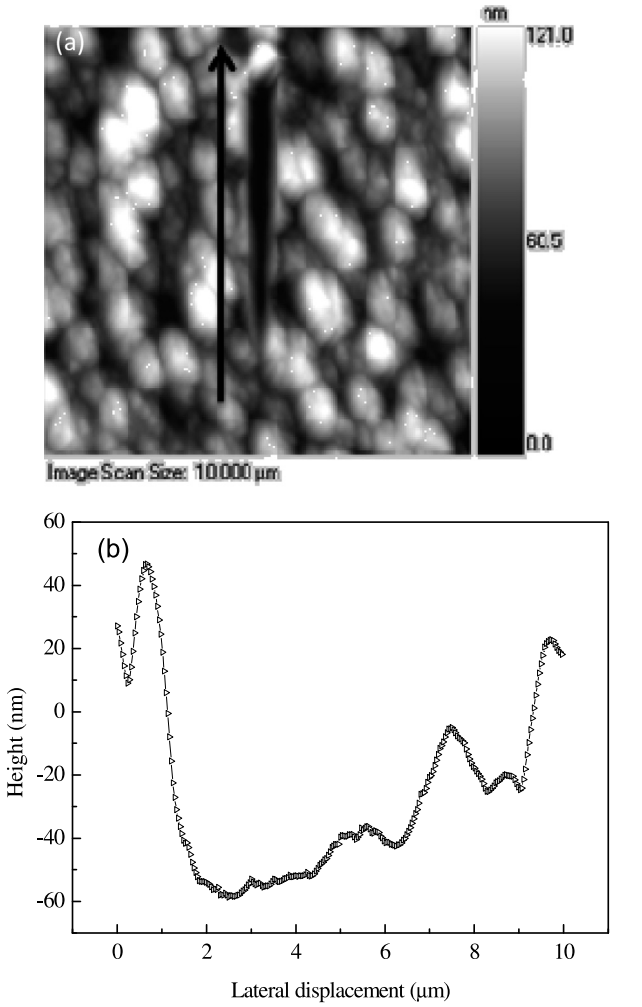

Fig. 9. (a) AFM image of residual scratch after removing the load. No pile-up and sink-in effects observed on the sides of the scratch were confirmed from this image. (b) Scratch profile of the scratch (direction shown with an arrow mark).

References

1. J.D. Merchant, M. Cocievera, J. Electrochem. Soc. **143**, 4054 (1996)
2. T. Ota, K. Takahashi, Solid-State Electron. **16**, 1089 (1973)
3. M. Nishio, K. Hayashida, Q. Guo, H. Ogawa, Appl. Surf. Sci. **169**, 223 (2001)
4. Q. Guo, Y. Kume, Y. Fukuhara, T. Tanaka, M. Nishio, H. Ogawa, M. Hiratsuka, M. Tani, M. Hangyo, Solid State Commun. **141**, 188 (2007)
5. A. Leitenstorfer, S. Hunsche, J. Shah, M.C. Nuss, W.H. Knox, Appl. Phys. Lett. **74**, 1516 (1999)
6. K.N. Raju, R.P. Vijayalakshmi, R. Venugopal, D.R. Reddy, B.K. Reddy, Mater. Lett. **13**, 336 (1992)
7. C.H. Su, M.P. Volz, D.C. Gilles, F.R. Szofran, M.R. Lehoczky, J. Cryst. Growth **128**, 627 (1993)
8. M.R.H. Khan, J. Phys. D: Appl. Phys. **27**, 2190 (1994)
9. W.I. Tao, M. Jurkovice, I.W. Wang, Appl. Phys. Lett. **64**, 1848 (1994)
10. B. Maiti, S. Gupta, S. Chaudhuri, A.K. Pal, Thin Solid Films **239**, 104 (1994)

11. K. Wolf, H. Stanzl, A. Naumov, H.P. Wagner, W. Kuhn, B. Kahn, W. Gebhardt, J. Cryst. Growth **138**, 412 (1994)
12. M. Neumann-Spallart, C. Konigstein, Thin Solid Films **265**, 33 (1995)
13. B. Bozzini, C. Lenardi, N. Lovergine, Mater. Chem. Phys. **66**, 219 (2000)
14. Y. Jun, K.J. Kim, D. Kim, Met. Mater. **5**, 279 (1999)
15. S. Arico, D. Silvestro, P.L. Antonucci, N. Giodano, V. Antonucci, Adv. Perform. Mater. **4**, 115 (1997)
16. A.A. Ibrahim, Vacuum **81**, 527 (2006)
17. T. Mahalingam, V.S. John, S. Rajendran, P.J. Sebastian, Semicond. Sci. Technol. **17**, 465 (2002)
18. B.M. Basol, V.K. Kapur, Thin Solid Films **165**, 237 (1988)
19. S.M. Patel, N.G. Patel, Mater. Lett. **2**, 131 (1983)
20. G.K. Rao, K.V. Bangera, G.K. Shivakumar, Vacuum **83**, 1485 (2009)
21. G. Purçek, E. Bacaksız, I. Miskioğlu, J. Mat. Process. Technol. **198**, 202 (2008)
22. R. Saha, W.D. Nix, Acta Mater. **50**, 23 (2002)
23. S.U. Jen, T.C. Wu, Thin Solid Films **492**, 166 (2005)
24. A. Portinha, V. Teixeire, J.O. Carneiro, S.N. Dup, R. Shmegera, C.J. Tavares, Surf. Coat. Technol. **200**, 765 (2005)
25. S. Simunkova, O. Blahova, I. Stepanek, J. Mater. Process. Technol. **133**, 189 (2003)
26. T.H. Fang, W.J. Chang, Microelectron. Eng. **65**, 231 (2003)
27. J.O. Carneiro, V. Teixeira, A. Portinha, S.N. Dub, R. Shmegera, Rev. Adv. Mater. Sci. **7**, 83 (2004)
28. E.R. Shaaban, I. Kansal, S.H. Mohamed, J.M.F. Ferreira, Physica B: Condens. Matter **404**, 3571 (2009)
29. R. Swanepoel, J. Phys. E: Sci. Instrum. **16**, 121 (1983)
30. R. Swanepoel, J. Phys. E: Sci. Instrum. **17**, 896 (1984)
31. E.E. Khawaja, M.A. Al-Daous, S.M.A. Durrani, M.F. Al-Kuhaili, Thin Solid Films **485**, 16 (2005)
32. E.A. Davis, N.F. Mott, Philos. Mag. **22**, 903 (1970)
33. E.A. Fagen, H. Fritzsche, J. Non-Cryst. Solids **2**, 180 (1970)
34. E.R. Shaaban, M. Abdel-Rahman, E.S. Yousef, M.T. Dessouky, Thin Solid Films **515**, 3810 (2007)
35. M.G. Krishna, A.K. Bhattacharya, Mater. Sci. Eng. B **86**, 41 (2001)
36. M.S.R.N. Kiran, M.G. Krishna, K.A. Padmanabhan, Appl. Surf. Sci. **255**, 1934 (2008)
37. F. Yakuphanoglu, M. Sekerci, A. Balaban, Opt. Mater. **27**, 1369 (2005)
38. T. Mahalingam, V.S. John, S. Rajendran, G. Ravi, P.J. Sebastian, Surf. Coat. Technol. **155**, 245 (2002)
39. W.C. Oliver, G.M. Pharr, J. Mater. Res. **7**, 1564 (1992)
40. W.C. Oliver, G.M. Pharr, J. Mater. Res. **19**, 3 (2004)
41. L.I. Berger, *Semiconductor Materials*, 1st edn. (CRC Press, New York, 1996)
42. S.E. Grillo, H. Glénat, T. Tite, O. Pages, O. Maksimov, M.C. Tamargo, Appl. Phys. Lett. **93**, 081901 (2008)
43. S. Simunkova, O. Blahova, I. Stepanek, J. Mater. Process. Technol. **133**, 189 (2003)
44. K. Durst, M. Goken, G.M. Pharr, J. Phys. D: Appl. Phys. **41**, 074005 (2008)
45. N.A. Fleck, G.M. Muller, M.F. Ashby, J.W. Hutchinson, Acta Metall. Mater. **42**, 475 (1994)
46. N.A. Fleck, J.W. Hutchinson, Adv. Appl. Mech. **33**, 295 (1997)
47. W.D. Nix, H. Gao, J. Mech. Phys. Solids **46**, 411 (1998)
48. M.F. Ashby, Philos. Mag. **21**, 399 (1970)